JOURNAL OF GUIDANCE, CONTROL, AND DYNAMICS
Vol. 26, No. 3, May–June 2003

Integrated Hardware Investigations of Precision Spacecraft Rendezvous Using the Global Positioning System

Takuji Ebinuma,* Robert H. Bishop,† and E. Glenn Lightsey‡
University of Texas, Austin, Texas 78712

A closed-loop spacecraft rendezvous simulation facility was constructed and configured to evaluate a newly developed relative navigation algorithm that processes the observables of the global positioning system. The primary objective of this effort is to establish the performance of the integrated guidance and navigation architecture for autonomous rendezvous in low Earth orbit. A fundamental component of the relative navigation system is a real-time recursive extended Kalman filter. To achieve very precise relative navigation, the filter processes double-differenced carrier-phase measurements. Based on the filter state, all of the maneuvers are computed onboard by solving the Lambert targeting problem. The closed-loop simulation investigations show that 3.5 cm or less relative positioning accuracy and 1.0 mm/s relative velocity estimation accuracy are achievable in the absence of multipath. With these highly accurate relative navigation results, coordinated and autonomous rendezvous maneuvers become possible.

Introduction

AUTONOMOUS rendezvous and capture is a key technology for low-Earth-orbit (LEO) applications that involve the International Space Station (ISS). An example of this type of application is an unmanned autonomous orbit transfer vehicle for expendable resupply of the ISS. A system of this type has the potential to reduce operational costs and simultaneously increase reliability and safety. Accurate real-time knowledge of relative position and velocity is one of the essential requirements for autonomous navigation and onboard targeting. The global positioning system (GPS) observables can be applied advantageously to relative navigation for two receivers with communication links between them. To achieve very precise relative navigation, double-difference carrier-phase measurements are commonly employed for ground-based activities. Space-based GPS relative navigation, however, differs from the conventional ground-based differential GPS approach in which at least one stationary receiver is usually located at a known position and navigation is performed with respect to the known station. In space-based applications, the positions of both vehicles may not be well known initially, and the vehicles are not stationary. In this paper, the application of double-differenced carrier-phase measurements is investigated for on-orbit navigation.

Much of the early work in the space-based GPS relative navigation field utilized only software simulation employing numerically generated GPS measurements.[1–5] This situation was due mainly to the lack of availability of spaceborne GPS receivers and testing equipment for the space dynamic environment. More recently, hardware-in-the-loop (HWIL) experiments have been reported using GPS signal generators.[6–9] In those experiments, the simulator generates the GPS signal received in the LEO environment, and the GPS measurements are provided by actual spaceborne GPS receivers connected to the simulator rf outputs. Although representing a step forward by utilizing hardware for GPS signal generation, all of the early HWIL experiments were open-loop experiments. Open-loop tests can provide some information about the basic performance of a navigation system, but they are limited to scripted trajectories that do not allow for control of the vehicles based on the navigation state. Rendezvous operations require precise relative navigation, but this alone is insufficient to allow autonomous on-orbit operations. The guidance algorithm relies on the navigation state and must operate in concert with the navigation system in a real-time mode.

One of the objectives of this research is to extend the HWIL experimentation to include a closed-loop integrated guidance and navigation architecture to establish the capabilities of on-orbit autonomous rendezvous operations using the GPS receivers as the only navigation sensors. Ebinuma et al.[10] presented the first closed-loop hardware simulation results of spacecraft rendezvous using a STR4670 GPS signal generator. In that experiment, however, only one GPS receiver was available; hence, one spacecraft (the passive vehicle) was not controlled in real time. The navigation filter read a RINEX-like log file for the passive vehicle, and only the observations of the active vehicle were supplied by the receiver in real time. A two receiver capability has since been developed, and the extension of the previous results to include closed-loop rendezvous hardware experiments with two GPS receivers is presented in this paper. The technical issues surrounding the integration of guidance and navigation in a real-time HWIL test are also investigated to ensure that no practical issues (such as timing mismatch) are overlooked.

Only a brief introduction to the filter algorithms is presented in this paper. More complete mathematical definitions and relative navigation algorithms are presented elsewhere by Ebinuma.[11]

Relative Navigation Architecture

Figure 1 shows the architecture of GPS-based spacecraft rendezvous system. We assume that a GPS receiver is mounted on each vehicle and that a communication link is used to pass GPS measurements from the target vehicle to the chaser vehicle. The chaser vehicle is actively maneuvering, while the target vehicle is passive. The centralized relative navigation filter on the chaser processes pseudorange and double-differenced carrier-phase measurements from both receivers concurrently. Because the vehicles are orbiting near each other, the GPS signal errors from the common GPS satellites and the perturbation errors are significantly correlated. When the correlated measurements are processed concurrently, the filter can provide more accurate relative state estimates than two independent navigation filters. Based on the target and chaser filter states, all of the targeting maneuvers are computed onboard by solving the Lambert targeting problem. This targeting algorithm requires absolute state information of both the target and chaser. To achieve

Received 14 May 2002; revision received 25 October 2002; accepted for publication 2 January 2003.

*Research Engineer, Center for Space Research, 3925 West Braker Lane, Suite 200, Austin, TX 78759. Member AIAA.
†Professor, Department of Aerospace Engineering and Engineering Mechanics. Associate Fellow AIAA.
‡Assistant Professor, Department of Aerospace Engineering and Engineering Mechanics. Senior Member AIAA.

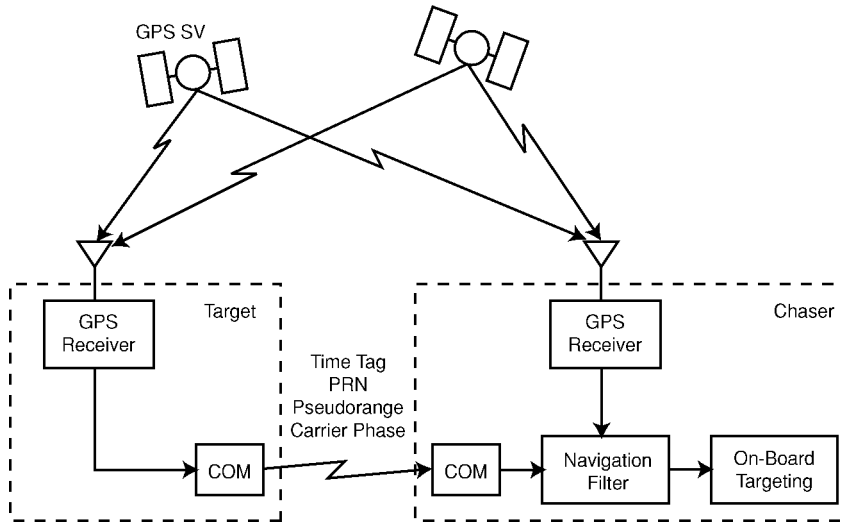

Fig. 1 GPS relative navigation architecture.

accurate absolute solutions, the receiver clock errors, ionospheric path delay, and ephemeris errors are also estimated as part of the filter state by processing pseudorange measurements, even though the effects of those error sources are conveniently eliminated from the relative navigation solutions by taking differential-phase measurements. Details of the filter design and onboard targeting algorithms will be discussed in the following sections.

Filter Model Descriptions

This section describes the nonlinear equations of the satellite motion and the GPS measurements used in the extended Kalman filter (EKF) algorithm (see Ref. 12). These nonlinear models are then linearized about the current filter state only for the covariance update.

Spacecraft Equations of Motion

The relative navigation filter utilizes a detailed inertial acceleration model for real-time state propagation. Many relative navigation applications utilize Hill's equations. Filter implementations using Hill's equations are less complex, but do not provide the necessary accuracy required from the application. The inertial acceleration model is also readily expandable to rendezvous applications in highly elliptical orbit, which is a subject for future investigations.

The spacecraft equations of motion are written as

$$\frac{\mathrm{d}^2\boldsymbol{r}}{\mathrm{d}t^2} = \boldsymbol{a} \tag{1}$$

where $\boldsymbol{r}$ and $\boldsymbol{a}$ are the satellite position and acceleration vectors, respectively. The total acceleration vector is defined as

$$\boldsymbol{a} = \boldsymbol{a}_E + \boldsymbol{a}_D + \boldsymbol{a}_U \tag{2}$$

where $\boldsymbol{a}_E$ is the Earth's gravity acceleration, $\boldsymbol{a}_D$ is the atmospheric drag acceleration, and $\boldsymbol{a}_U$ is the remaining unmodeled acceleration vectors.

The Earth's gravitational acceleration vector $\boldsymbol{a}_E$ is given by the gradient of the geopotential function ψ as

$$\boldsymbol{a}_E = \nabla\psi \tag{3}$$

Expressed in terms of the satellite's radius r, latitude ϕ, and longitude λ, here ψ is given by

$$\psi = \frac{\mu_E}{r}\left\{1 - \sum_{n=2}^{N}\sum_{m=0}^{n}\left(\frac{R_E}{r}\right)^n P_{nm}(\sin\phi)[C_{nm}\cos(m\lambda) + S_{nm}\sin(m\lambda)]\right\} \tag{4}$$

where R_E is the mean equatorial radius of the Earth, $P_{nm}(\sin\phi)$ is the associated Legendre function, S_{nm} and C_{nm} are sectorial and tesseral harmonic coefficients, respectively, and N is maximum degree included in the expansion. A more detailed description is found by Vallado.[13] Only the second-order zonal harmonic coefficient, $J_2(=-C_{20})$, is selected for the gravitational acceleration model in the filter. Neglecting higher-order gravitational harmonics terms leads to periodic disturbances. The unmodeled acceleration vector $\boldsymbol{a}_U$ is added to the navigation system to absorb the acceleration errors created by these disturbances and is part of the filter state vector.

The atmospheric drag acceleration vector $\boldsymbol{a}_D$ is modeled as a drag force in the direction of the relative wind vector acting on a constant surface of the spacecraft. The basic equation for aerodynamic drag acceleration is

$$\boldsymbol{a}_D = -\tfrac{1}{2}(C_D A/m)\varrho v_{\mathrm{rel}}^2(\boldsymbol{v}_{\mathrm{rel}}/|\boldsymbol{v}_{\mathrm{rel}}|) \tag{5}$$

where C_D is the drag coefficient, A is the reference surface area of the satellite, m is the mass of the satellite, and ϱ is the atmospheric density. The velocity vector relative to the rotating atmosphere is

$$\boldsymbol{v}_{\mathrm{rel}} = \dot{\boldsymbol{r}} - \boldsymbol{\omega}_E \times \boldsymbol{r} \tag{6}$$

where $\boldsymbol{\omega}_E$ is the Earth's rotation vector. To predict the atmospheric density, the filter uses an exponential atmosphere density model, in which the air density varies as

$$\varrho = \varrho_0 \exp[-(h - h_0)/H] \tag{7}$$

where ϱ_0 is reference density, h is actual altitude above a reference ellipsoid, h_0 is reference altitude, and H is scale height. Because the exponential model gives a daily average density, it cannot express the diurnal changes in the day-side and night-side on the orbit. The drag coefficient correction Δ_D that is added to the filter state vector to compensate for these modeling errors, as well as the variation from the nominal value $\bar{C}_D$ of the drag coefficient, is as follows:

$$C_D = (1 + \Delta_D)\bar{C}_D \tag{8}$$

Both the unmodeled acceleration and drag coefficient correction states utilize exponentially correlated random variable (ECRV) models. In a discrete-time formulation, a state x_k modeled as an ECRV can be described with a time constant τ and the standard deviation σ as

$$x_{k+1} = \alpha x_k + q\eta_k \tag{9}$$

where the scalar state transition is given by

$$\alpha = \exp[-(t_{k+1} - t_k)/\tau] \tag{10}$$

and η_k is a zero mean, unit variance random variable. The process noise covariance

$$q = \sigma\sqrt{1-\alpha^2} \tag{11}$$

appears in the filter process noise vector.

GPS Observables

Although most GPS receivers provide least-square (or point-fix) solutions of the receiver position and the receiver clock bias, the navigation filter processes the GPS observables directly. The pseudorange model between the GPS satellite S and the receiver R is

$$P_R^S(t_R) = \rho_R^S(t_R) + c\Delta t_R - c\Delta t^S + \Delta E_R^S + \Delta I^S + \xi_R^S \tag{12}$$

where $\rho_R^S(t_R)$ is the range computed on the basis of the broadcast ephemeris and the receiver position at t_R, c is the speed of light, and Δt_R and Δt^S are receiver and GPS satellite clock errors, respectively. In addition to the clock errors, the actual pseudorange measurement is affected by the ionospheric delay ΔI^S, broadcast ephemeris error ΔE_R^S, and random noise ξ. Note that the tropospheric delay is not included because the spacecraft is assumed to orbit above the troposphere. Because the selective availability (SA) was removed on 1 May 2000, SA clock dither and ephemeris manipulation errors are also not included as part of the measurement errors. The effect of multipath is not included in the current filter design, but should be considered in future work. Similarly, the carrier-phase measurement model can be expressed as

$$\lambda\Phi_R^S(t_R) = \rho_R^S(t_R) + c\Delta t_R - c\Delta t^S + \Delta E_R^S - \Delta I^S + \lambda N + \zeta_R^S \tag{13}$$

where λ is the wave length of the L1 carrier signal. The carrier phase only differs from the pseudorange in Eq. (12) by the sign of the ionospheric delay, the random noise ζ, and the integer ambiguity N, multiplied by λ. More detailed model descriptions of GPS observables are found by Leick.[14]

GPS Measurement Biases

The navigation filter estimates each individual range bias source in Eqs. (12) and (13) to achieve more accurate spacecraft filter state estimation. The normalized receiver clock bias Δt_R, denoted by b, is given by

$$b = c\Delta t_R \tag{14}$$

The receiver clock model is then defined by

$$\dot{b} = f + w_f \tag{15}$$

$$\dot{f} = w_g \tag{16}$$

where f is the clock drift and w_f and w_g are the zero mean Gaussian white noise.

The GPS satellite ephemeris and clock corrections are regularly predicted by the operational control segment and uploaded to the satellites in the form of orbit elements and curve fit parameters. The parameters are then included as part of the navigation message. User receivers utilize the parameters to estimate the satellite coordinates and clock corrections. The errors in the broadcast ephemeris yield the range bias denoted by ΔE_R^S in Eqs. (12) and (13). Because the broadcast ephemeris error slowly changes while the GPS satellite is visible, it is treated as an ECRV in the navigation filter.

The ionosphere introduces a path-dependent delay in the GPS measurements. Denote I_V as a ionospheric range error for the L1 carrier signal along the local vertical. In the navigation filter, I_V is modeled as

$$I_V = (1 + \Delta_{IV})\bar{I}_V \tag{17}$$

where the ionospheric delay correction Δ_{IV} is added to the filter state vector to absorb the variation from a nominal delay value $\bar{I}_V$ and is treated as an ECRV. The ionospheric delay ΔI^S for each GPS satellite is then computed by an obliquity equation,

$$\Delta I^S = \frac{2.04 I_V}{\sqrt{\sin^2 E + 0.076} + \sin E} \tag{18}$$

where E is the elevation angle of the signal path from the GPS satellite S with respect to the local horizon.

Double-Differenced Carrier Phase

In conventional ground-based relative positioning applications, the coordinate of an unknown receiver position is determined with respect to a well-known point, which is stationary for most cases. In space-based relative navigation applications, however, both the target and chaser receivers are orbiting around the Earth. The spacecraft initial positions are not initially well known, and they are moving with respect to one another. Relative positioning can be performed either with pseudorange or carrier-phase measurements. In the relative navigation filter, double-differenced carrier-phase measurements are used to improve the accuracy of relative state estimates.

Denote the target and chaser spacecraft by subscripts A and B, respectively, and the two GPS satellites by superscripts j and k. The phase difference requires simultaneous observations from both the target and chaser receivers. Simultaneity means that the GPS measurement time tag for the two receivers are the same. When it is assumed that such simultaneous observations exist, the double-differenced measurements are defined as

$$\lambda\Phi_{AB}^{jk} = \lambda\Phi_A^j - \lambda\Phi_B^j - \lambda\Phi_A^k + \lambda\Phi_B^k \tag{19}$$

Assume that the two user spacecraft are close enough so that the signal path from each GPS satellite is almost the same. Thus, the GPS satellite-related errors, such as ionospheric delay, broadcast emphemeris error, and satellite clock error, are canceled when taking the double difference. When Eq. (13) is substituted into Eq. (19), the double-differenced carrier-phase measurement is given by

$$\lambda\Phi_{AB}^{jk} = \rho_{AB}^{jk} + \lambda N_{AB}^{jk} + \zeta_{AB}^{jk} \tag{20}$$

The double-differenced integer ambiguity λN_{AB}^{jk} in Eq. (20) is part of filter state vector, and its estimate is a real number. Because the integer ambiguity is taking a fixed constant value while the carrier phase is observed (if a cycle slip does not occur), the double-differenced integer ambiguity is also a fixed constant. Although it is known to be constant, a small amount of process noise is given to allow for innovations in the bias value to occur over time.

Filter State Vector

The filter estimates a state vector $\boldsymbol{X}$, which consists of the two user spacecraft position and velocity vectors and receiver clock biases, as well as the GPS measurement errors. The state vector used in the filter is

$$\boldsymbol{X} = [\boldsymbol{X}_A;\quad \boldsymbol{X}_B;\quad \Delta_{IV};\quad \boldsymbol{X}_E;\quad \boldsymbol{X}_N] \tag{21}$$

where

$\boldsymbol{X}_A$ = target spacecraft and receiver clock bias state
$\boldsymbol{X}_B$ = chaser spacecraft and receiver clock bias state
Δ_{IV} = scalar ionospheric delay correction
$\boldsymbol{X}_E$ = broadcast ephemeris biases
$\boldsymbol{X}_N$ = double-differenced integer ambiguities

Here and subsequently, the notation $[\boldsymbol{a};\ \boldsymbol{b}]$ is used as a shorthand for the more cumbersome $[\boldsymbol{a}^T,\ \boldsymbol{b}^T]^T$.

For each vehicle, the spacecraft and receiver clock bias state is defined as

$$\boldsymbol{X}_i = [\boldsymbol{r};\quad \dot{\boldsymbol{r}};\quad \Delta_D;\quad \boldsymbol{a}_U;\quad b;\quad f]_i, \qquad i = A, B \tag{22}$$

Note that the filter estimates the position and velocity of the center of mass and that the antenna phase center is assumed to coincide

Table 1 Summary of the filter state

State vector	Number of states
$\boldsymbol{X}_A$	
Target position	3
Target velocity	3
Target drag coefficient correction	1
Target unmodeled acceleration	3
Target receiver clock bias	1
Target receiver clock drift	1
$\boldsymbol{X}_B$	
Chaser position	3
Chaser velocity	3
Chaser drag coefficient correction	1
Chaser unmodeled acceleration	3
Chaser receiver clock bias	1
Chaser receiver clock drift	1
Δ_{IV}, ionospheric delay correction	1
$\boldsymbol{X}_E$, broadcast ephemeris errors	n
$\boldsymbol{X}_N$, double-difference ambiguity	$n-1$
Total size	$25+2n-1$

with the center of mass. No attitude determination is implemented in the current filter design. The broadcast ephemeris bias state vector $\boldsymbol{X}_E$ is composed of ΔE_R^S of each GPS satellite. When n satellites are commonly visible from both the chaser and target vehicles, the length of $\boldsymbol{X}_E$ becomes n. Similarly, $\boldsymbol{X}_N$ is composed of a double-differenced integer ambiguity λN_{AB}^{jk} for each double-differenced carrier-phase measurement. From n carrier phase measurements, $(n-1)$ linearly independent double-differenced measurements can be taken. Table 1 summarizes the filter state vector components and their dimensions. The total length of the state vector becomes $25+2n-1$.

The filter state is basically composed of two inertial states of the target and chaser vehicles. The relative state vector $\boldsymbol{X}_{\text{rel}}$ of the chaser spacecraft with respect to the target spacecraft is then obtained by differencing the inertial state estimates as

$$\boldsymbol{X}_{\text{rel}} = \boldsymbol{X}_B - \boldsymbol{X}_A \tag{23}$$

If we denote the difference between the true and estimated states by $\boldsymbol{e}$, the relative state error covariance matrix $\boldsymbol{P}_{\text{rel}}$ is expressed as

$$\begin{aligned}\boldsymbol{P}_{\text{rel}} &= E\left\{\boldsymbol{e}_{\text{rel}}\boldsymbol{e}_{\text{rel}}^T\right\}\\ &= E\left\{(\boldsymbol{e}_B-\boldsymbol{e}_A)(\boldsymbol{e}_B-\boldsymbol{e}_A)^T\right\}\\ &= \boldsymbol{P}_A+\boldsymbol{P}_B-\boldsymbol{P}_{AB}-\boldsymbol{P}_{BA}\end{aligned} \tag{24}$$

where $\boldsymbol{P}_A$, $\boldsymbol{P}_B$, $\boldsymbol{P}_{AB}$, and $\boldsymbol{P}_{BA}$ $(=\boldsymbol{P}_{AB}^T)$ are the state error covariance block matrices corresponding to the spacecraft state vectors. Processing double-differenced measurements is beneficial for simultaneous estimation of two inertial states because it leads to cross correlation between the two inertial states and, therefore, decreases the error covariance of the relative state vector in Eq. (24).

Observation Vector

At every sampling time, the filter process both the nondifferenced pseudorange and double-differenced carrier phase measurements. The observation vector $\boldsymbol{Y}$ is defined by

$$\boldsymbol{Y} = [\boldsymbol{Y}_{\text{PR},A};\quad \boldsymbol{Y}_{\text{PR},B};\quad \boldsymbol{Y}_{\text{DD}}] \tag{25}$$

where $\boldsymbol{Y}_{\text{PR},A}$ and $\boldsymbol{Y}_{\text{PR},B}$ are the pseduorange measurement vectors received by the target and chaser, respectively, and $\boldsymbol{Y}_{\text{DD}}$ is the double-differenced carrier-phase measurement vector. When n satellites are commonly visible from both the target and chaser vehicle, the length of $\boldsymbol{Y}$ becomes $(3n-1)$.

Note that the filter needs to process nondifferenced pseudorange measurements because some of the filter states, such as the receiver clock bias and the broadcast ephemeris error, are not (or are very weakly) observable with double-differenced measurements alone.

State Estimation Algorithms

The state estimation algorithms of the relative navigation filter consist of the following four major processes. In addition to the general EKF propagation and measurement update processes, a bookkeeping process of the state vector is required due to the changes of the number of visible satellites.

1) Maintenance process consists of maintaining the length of the states and the size of state error covariance matrices of the broadcast ephemeris errors and double-differenced integer ambiguities corresponding to the number of commonly visible GPS satellites from both the chaser and target.

2) Measurement update process consists of correcting the state vector and the state error covariance matrix to include the effects of the current measurement taken from the GPS satellites. The GPS satellites considered include only those that have been continuously observed since the last initialization process.

3) Initialization process consists of initializing the state vector and the state error covariance matrix corresponding to the recently locked-on GPS satellites.

4) Propagation process consists of propagating the state vector and state error covariance matrix from the current measurement time to the next.

Onboard Targeting Algorithms

Based on the target and chaser filter states, all of the targeting maneuvers are computed onboard by solving the Lambert targeting problem. Given two position vectors and the time of flight from one to the other, the Lambert algorithm gives the initial velocity that generates the orbit connecting the two positions. Because the Lambert problem is defined in a simple two-body environment, the resulting impulsive maneuver vector $\Delta\boldsymbol{V}$ cannot take the spacecraft to the desired final position under the effects of disturbing forces. However, an iterative method is employed to implement the Lambert algorithm to compute $\Delta\boldsymbol{V}$, which achieves an accurate final positioning within a given threshold ϵ in the real-world environment.

1) Given filter state vectors of the target $\boldsymbol{X}_A(t_m)$ and the chaser $\boldsymbol{X}_B(t_m)$ at the time of ignition t_m, propagate the target state to the final time t_f with the filter acceleration model and obtain the estimated final target state $\boldsymbol{X}_A(t_f)$.

2) Solve the Lambert problem with the time of flight $\Delta t = t_f - t_m$, the initial position $\boldsymbol{X}_B(t_m)$, and the final position $\boldsymbol{X}_A(t_f)$ to obtain $\Delta\boldsymbol{V}$.

3) Propagate the chaser position $\boldsymbol{X}_B(t_m)$ with $\Delta\boldsymbol{V}$ to the final time and obtain the estimated chaser final position $\boldsymbol{X}_B(t_f)$.

4) Compute the error in the final position $\Delta\boldsymbol{X} = \boldsymbol{X}_B(t_f) - \boldsymbol{X}_A(t_f)$.

5) If $|\Delta\boldsymbol{X}| > \epsilon$, set the final target position $\boldsymbol{X}_A(t_f) \leftarrow \boldsymbol{X}_A(t_f) - \Delta\boldsymbol{X}$ and go to step 2.

Simulation Setup

The HWIL GPS test facility was configured to test the relative navigation and onboard target algorithms in a real-time mode with two GPS Orion receivers. This section describes the test facility setup for the closed-loop rendezvous simulation.

Simulation Hardware

Figure 2 shows the GPS test facility, and Fig. 3 shows the HWIL system configuration for the closed-loop rendezvous simulation with two GPS receivers. The GPS L1 Coarse/Acquisition-code signal is simulated using a Spirent STR4760 simulator composed of one workstation (Compaq Alpha Station XP900) and one rf signal generator connected to the workstation via an Institute of Electrical and Electronics Engineers- (IEEE-) 488 control bus. The workstation controls the entire operation of the signal generator under user-specific scenarios. The signal generator has 2 rf outputs (16 channels each) and is capable of simulating the GPS signals received by 2 user vehicles simultaneously. From each rf output line, the simulated GPS signal is then sent to a Mitel GPS Orion receiver through

a coaxial cable. The GPS Orion is a sample receiver design released by Mitel Semiconductor. The core components of the receiver are the GP2015 rf front end, GP2021 12-channel correlator, and ARM60 32-bit reduced instruction set computer processor. The major advantage of the GPS Orion receiver is the availability of the receiver source code and development environment. Because the receiver was originally designed for terrestrial applications, some modifications were required for operations in space dynamics environment. The two GPS Orion receivers used in this research (Fig. 4) were built and modified for space applications by Montenbruck et al. for their suborbital sounding rocket experiments.[15] Each receiver provides GPS measurements to the navigation computer, which runs the relative navigation filter and onboard targeting algorithms.

In addition to the STR4760 system, the closed-loop simulation requires the STR4762 remote control option that allows the simulation to be controlled by an external personal computer in real time. The external personal computer runs two satellite trajectory propagators simultaneously and provides position, velocity, and acceleration vectors of the two vehicles to the workstation every 100 ms through an IEEE-488 bus. Based on that motion data, the workstation calculates the pseudorange information used by the signal generator. The satellite trajectory simulation environment for the external personal computer employs the following acceleration models: 1) Earth's gravitational acceleration with the 30×30 joint gravity model-3, 2) atmospheric drag with the Marshall Engineering Thermosphere model, and 3) third-body perturbations due to the sun and the moon. The propagators are also capable of accepting ΔV vectors from the navigation personal computer through RS232 serial lines for real-time trajectory corrections.

Trajectory Propagator Settings

The target and chaser scenarios used in this paper are the same rendezvous scenarios designed for previous investigations.[10] The ISS was chosen as the target and assumed to be passive, and the automated transfer vehicle (ATV), a European unmanned service vehicle for the ISS, was the actively maneuvering chaser vehicle. Table 2 shows the initial target and chaser state vectors. The ISS orbit was chosen to be a near circular in the inclination of 51.6 deg. The ATV was assumed to be in the same orbit and initially about 10 km behind the ISS in the along-track direction. Table 3 shows the physical parameters of the ISS and ATV used in the satellite trajectory propagators.

The closed-loop rendezvous simulation lasts 90 min. For the first 30 min, both the chaser and target are orbiting passively. The terminal intercept (TI) burn is applied at $T = 30$ min, and a total three

Table 2 ISS and ATV initial states

State	ISS	ATV
X position, m	$6.771358863E+6$	$6.771351472E+6$
Y position, m	0.000000000	$-0.006217690E+6$
Z position, m	0.000000000	$-0.007844773E+6$
X velocity, m/s	0.000000000	$0.011336325E+3$
Y velocity, m/s	$4.768073929E+3$	$4.768068724E+3$
Z velocity, m/s	$6.015812115E+3$	$6.015805548E+3$

Table 3 ISS and ATV parameters

Parameter	ISS	ATV
Drag coefficient	2.3	2.0
Reference area, m^2	2,000	20
Vehicle mass, kg	470,000	20,000

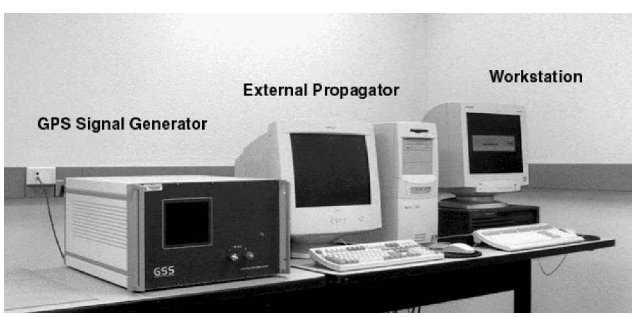

Fig. 2 GPS signal simulator.

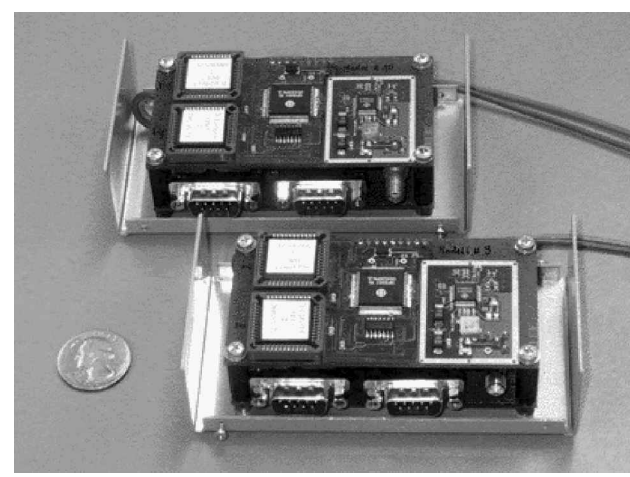

Fig. 4 GPS Orion receivers.

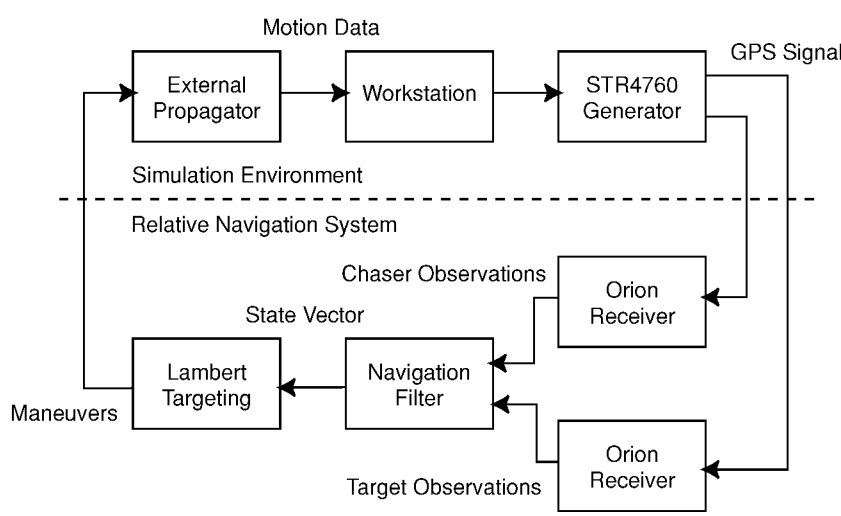

Fig. 3 HWIL system configuration.

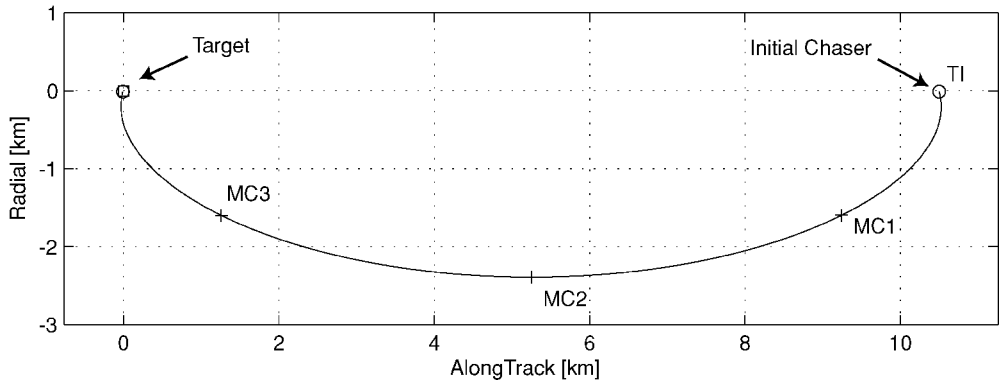

Fig. 5 Typical rendezvous trajectory.

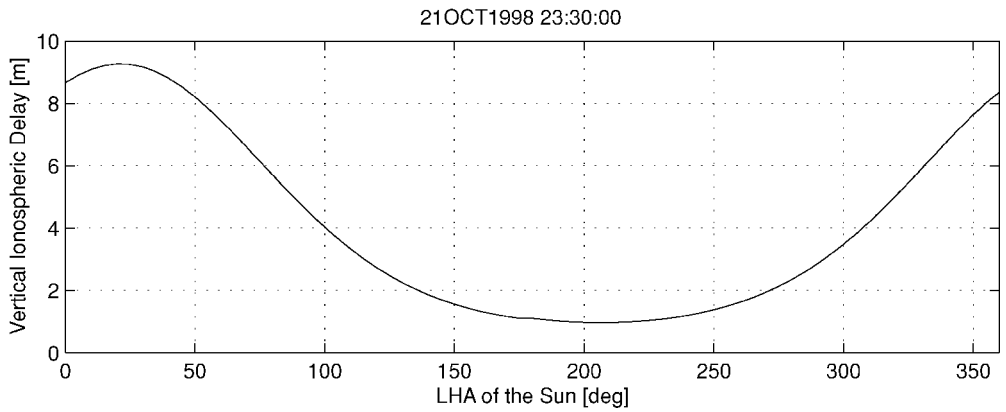

Fig. 6 Simulated ionospheric delay profile.

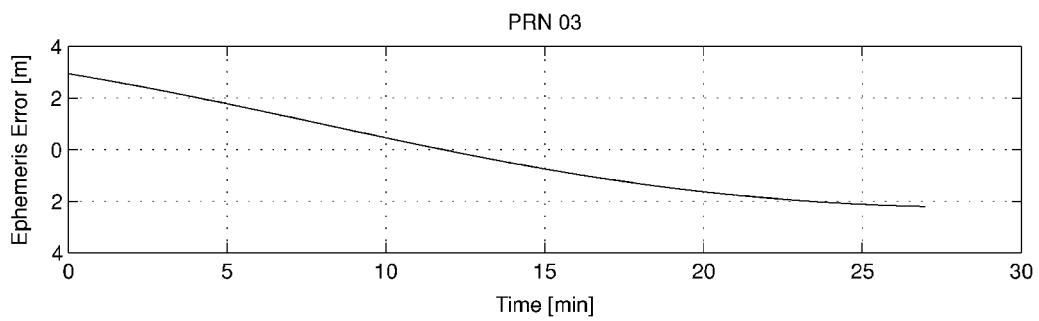

Fig. 7 Example of simulated ephemeris range error.

midcourse correction (MC) burns are executed every 15 min to reduce the final positioning error due to the perturbation forces and the thruster errors. Figure 5 shows an example rendezvous trajectory of the ATV relative to the ISS in the target-centered rotating frame. Because all of the TI and MC burns are computed based on the filter state vector, the chaser trajectory varies with each simulation.

Signal Simulator Settings

Based on the position, velocity, and acceleration vectors of the target and chaser vehicles sent from the external propagators, the STR4760 workstation calculates the pseudorange information used by the signal generator. The simulator settings used in this paper are also the same as those employed in previous investigations.[10] The GPS constellation is based on the YUMA almanac file of GPS week 980, which contains 27 active GPS satellites. The antenna boresight is assumed to point along the radial direction. The simulator is instructed to provide signals of all GPS satellites that are 0 deg above the local horizon, whereas the elevation mask of the Orion receiver is 10 deg. The ionospheric delay and broadcast ephemeris errors are intentionally added to the simulated GPS measurements. Figures 6 and 7 show typical range error profiles due to the ionospheric delay and broadcast ephemeris error, respectively.

Closed-Loop Simulation Results

Figure 8 shows the relative navigation error in the rendezvous simulation. In Fig. 8, the solid lines represent estimation errors and the dotted lines represent the corresponding standard deviation taken from the filter state error covariance matrix. The navigation filter is initialized based on the first position and velocity fix solutions obtained by the GPS receivers internally. This implies that no prior knowledge of position and velocity is required for the filter initialization. The "hot start" capability[16] implemented inside of the Orion receiver provides the first position fix solution within a couple of minutes after booting the receiver, whereas the time to first fix from "cold start" takes typically 8–10 min. The burn errors of 2.0 cm/s (1σ) in the burn direction and 0.2 cm/s (1σ) in the other directions were added in the chaser trajectory propagator. To compensate for the unmodeled dynamics due to the burn error, the state error covariance was intentionally increased based on the magnitude of the ΔV vector. If the magnitude of the computed ΔV is less than 2.0 cm/s, no MC burn is executed at that time.

Table 4 summarizes the relative navigation accuracy at the final approaching time ($T = 90$ minutes). The value of each relative state error is taken from the square root of the corresponding state error covariance, not the rms of the actual navigation errors. The row labeled

$\sqrt{[\lambda_{\max}(\boldsymbol{P})]}$ in Table 4 shows the square root of the largest eigenvalue of the state error covariance matrix. Because the 3×3 state error covariance matrices corresponding to the position and velocity state vectors represent 1σ error ellipsoids in a Cartesian coordinate system, the square root of the largest eigenvalue of the state error covariance matrix indicates the largest (worst) standard deviation of the state error, and the corresponding eigenvector indicates its direction. Figure 9 shows typical shapes of relative position state error covariance ellipses along the rendezvous trajectory. The closed-loop simulation results show that about 3.5-cm relative positioning accuracy and about 1.0-mm/s relative velocity estimation accuracy are achievable without multipath. Although the current filter setting provides somewhat larger relative velocity state error covariance than the actual rms values of the velocity errors, an early numerical investigation of Ebinuma[11] indicates that the process noise covariance should remain conservative to obtain unbiased relative position errors. The offsets in the relative position errors tend to be larger in a longer separation distance mainly due to the small difference of ionospheric path delays between the target and the chaser remaining in the double-differenced measurements.

Table 4 Relative state accuracy at final time

Direction	Position, cm	Velocity, mm/s
Radial	3.44	0.90
Along track	2.49	0.52
Cross track	2.46	0.69
$\sqrt{\lambda_{\max}(\boldsymbol{P})}$	3.50	1.02

Figure 10 shows the chaser absolute filter state errors. Although the ionospheric path delay and the broadcast ephemeris errors are intentionally added to the simulated GPS measurements, the absolute state errors plots show unbiased estimation errors. This is a good

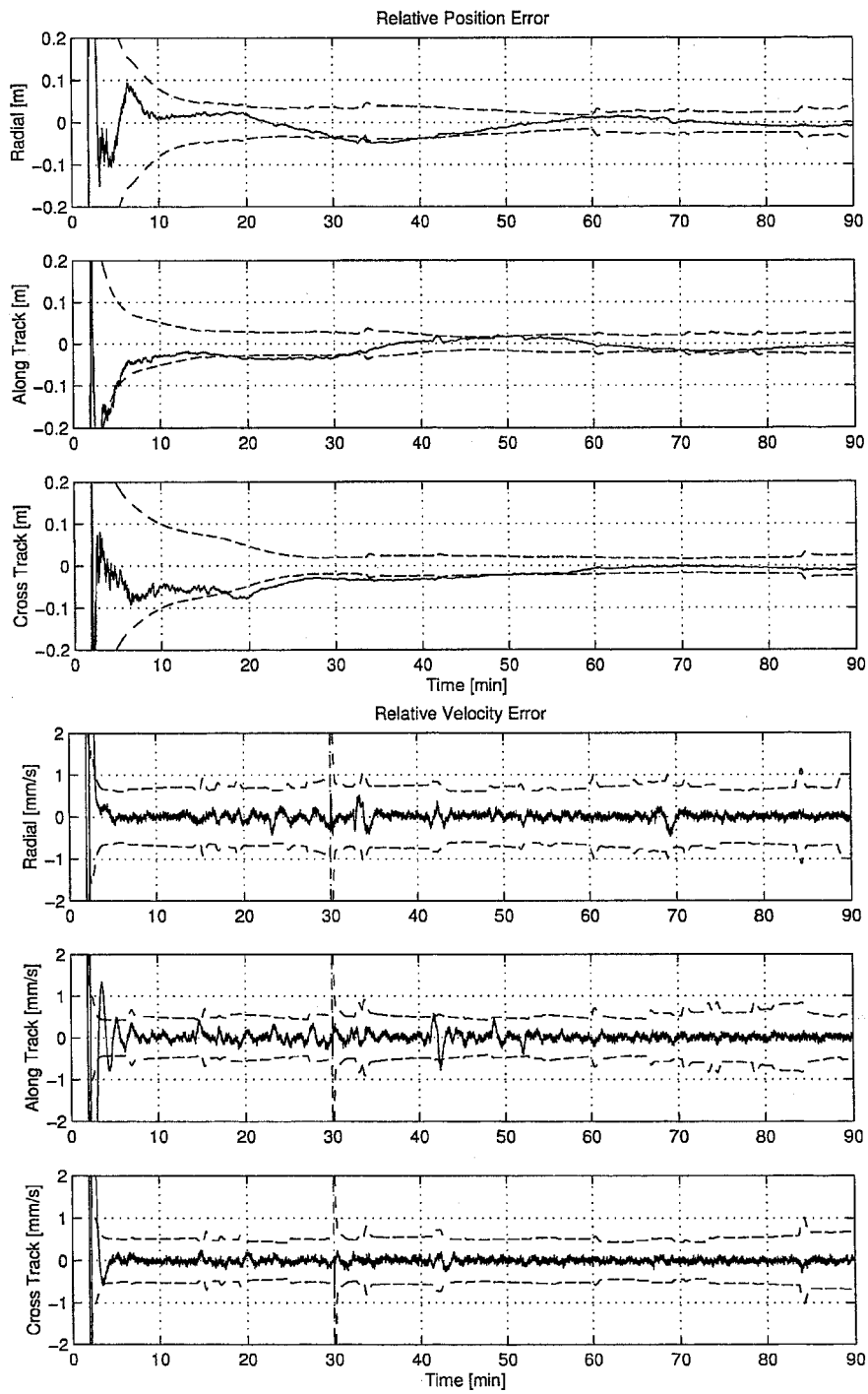

Fig. 8 Relative state accuracy.

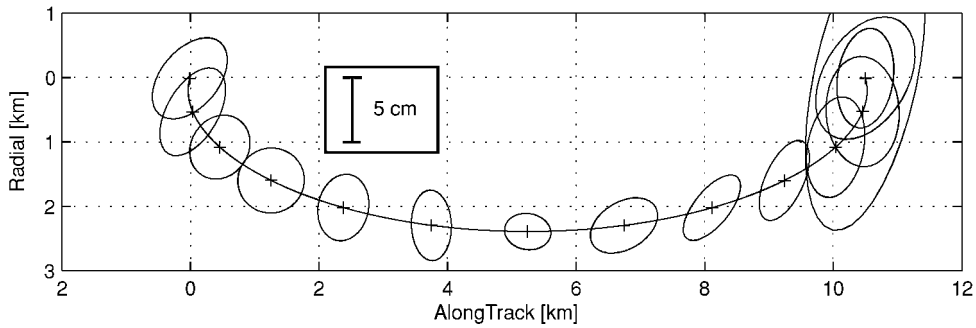

Fig. 9 Relative position state 1σ error ellipses.

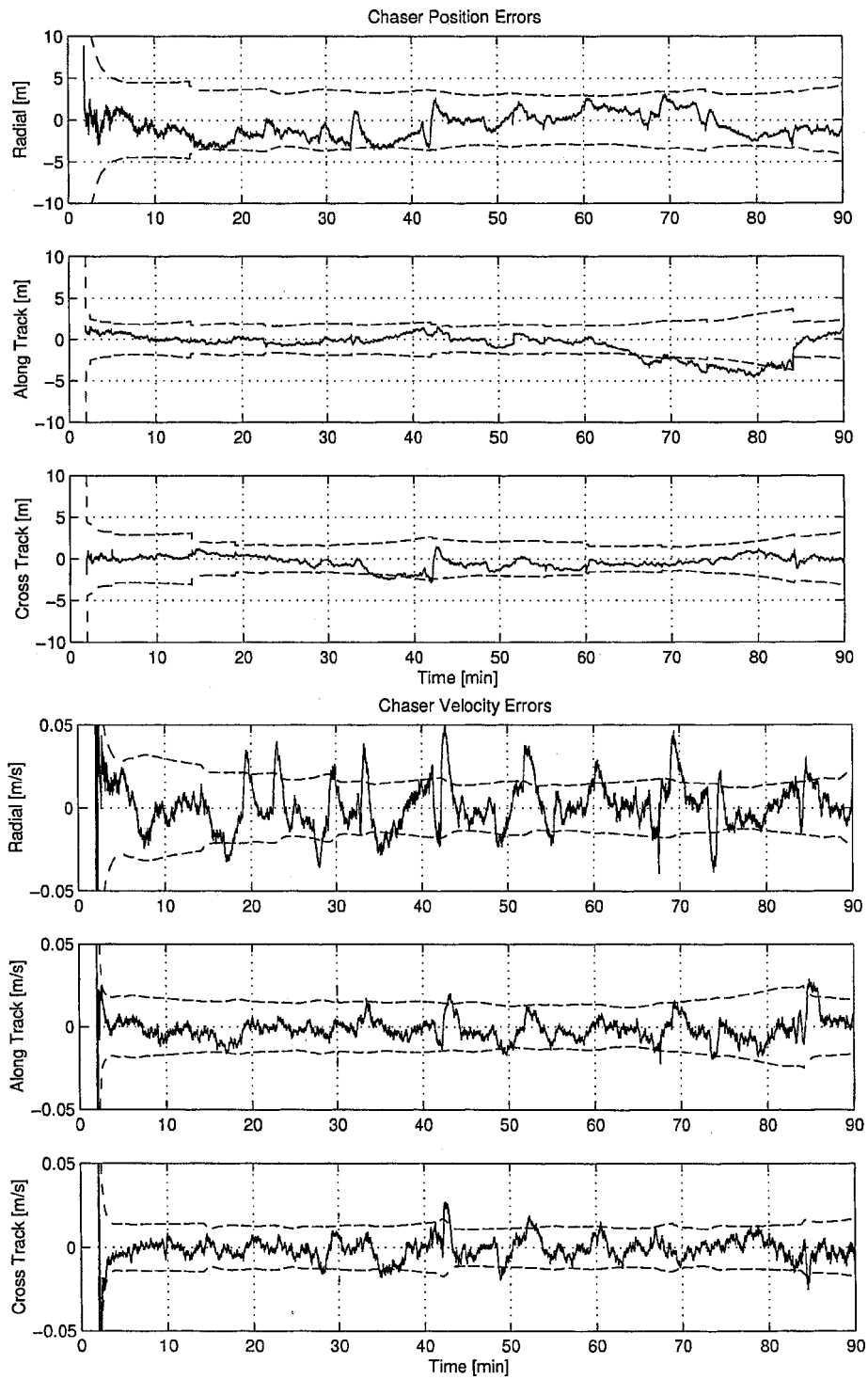

Fig. 10 Chaser absolute state accuracy.

indication that the auxiliary filter states, such as the ionospheric delay correction and the broadcast ephemeris errors, are successfully estimated. Also note that, in the previous HWIL experiment results with a Mitel Architect receiver presented by Ebinuma et al.,[10] there was an along-track position offset of up to 7 m due to the 1-ms time tagging error in the original Mitel receiver source code. This offset was fixed by Montenbruck et al.[15] and is no longer observed.

Because the main focus of this research is the hardware integration of the relative navigation and guidance systems, there is no Monte Carlo type analysis of the EKF performance presented in this paper. Rigorous numerical investigations for the optimal filter implementation may be found in an early investigation of Ebinuma.[11]

Conclusions

The HWIL GPS test facility was configured to perform active closed-loop simulations with two GPS Orion receivers, and the experiments has been successfully extended to include real-time integrated guidance and navigation for spacecraft rendezvous. All of the measurements taken from actual spaceborne GPS receivers are processed onboard, and the rendezvous maneuvers are computed and executed based on the filter navigation state vector in real time. Under LEO conditions with 10-km initial separation, the relative navigation filter provides relative state accuracy of 3.5 cm for positioning and 1.0 mm/s for velocity estimation without considering the effects of multipath and signal blockage.

The real-time rendezvous simulations between an unmanned resupply vehicle and the ISS were successfully demonstrated in the current configuration, but the scenario settings were simplified. For example, no signal blockage and multipath effects were considered in the simulation, although they are the main measurement error sources in the vicinity of large space structures. A multipath model and signal blockage based on the physical shape of the vehicles should be added to the simulation environment. It is also promising to consider utilizing measurements from auxiliary systems, such as inertial navigation systems and/or pseudolites, to remove the obstruction problem for space station approach navigation.

Although this paper has focused only on spacecraft rendezvous simulations, there are a number of applications in this area that could be considered. As another example of the GPS relative navigation applications, spacecraft formation flying would be an enabling technology for Earth mapping, synthetic aperture, and interferometry missions. The capability of formation flying is not investigated in this paper, but could be considered in future work.

Acknowledgments

This research was completed under NASA Goddard Space Flight Center (GSFC) Contract NAG5-9829. The authors thank Russell Carpenter of NASA GSFC for his support. The authors are grateful to Oliver Montenbruck at German Space Operation Center for his effort to modify the GPS Orion receiver software to work efficiently in the low-Earth-orbit dynamics environment and his collaboration during his stay at University of Texas Center for Space Research.

References

[1]Galdos, J., and Upadhyay, T. N., "A GPS Relative Navigation Filter for Automatic Rendezvous and Capture," *1993 National Technical Meeting*, Inst. of Navigation, Fairfax, VA, 1993, pp. 83–94.

[2]Zyla, L. V., and Montez, M. N., "Use of Two GPS Receivers in Order to Perform Space Vehicle Orbital Rendezvous," *ION GPS-93*, Inst. of Navigation, Fairfax, VA, 1993, pp. 301–312.

[3]Ambrosius, B. A. C., Hesper, E. T., and Wakker, K. F., "Application of the Global Positioning System for Hermes Rendezvous Navigation," *Journal of Guidance, Control, and Dynamics*, Vol. 16, No. 1, 1993, pp. 197–205.

[4]Frezet, M., Marcille, H., Pascal, V., and Pairot, J. M., "Relative GPS Navigation for ATV Rendezvous," *ION GPS-95*, Inst. of Navigation, Fairfax, VA, 1995, pp. 269–278.

[5]Cox, D. B., and Brading, J. D. W., "GPS Autonomous Relative Navigation and Time Transfer for Orbiting Space Vehicles," *ION GPS-95*, Inst. of Navigation, Fairfax, VA, 1995, pp. 217–228.

[6]Binning, P. W., "Absolute and Relative Satellite to Satellite Navigation Using GPS," Ph.D. Dissertation, Dept. of Aerospace Engineering Sciences, Univ. of Colorado, Boulder, CO, April 1997.

[7]Binning, P. W., and Galysh, I., "Satellite to Satellite Relative Navigation Using GPS Pseudoranges," *1997 National Technical Meeting*, Inst. of Navigation, Fairfax, VA, 1997, pp. 407–416.

[8]Kawano, I., Mokuno, M., and Kasai, T., "Relative GPS Navigation for an Automated Rendezvous Docking Test Satellite ETS-VII," *ION GPS-97*, Inst. of Navigation, Fairfax, VA, 1997, pp. 707–715.

[9]D'Souza, C., Bogner, A., Brand, T., Tsukui, J., Koyama, H., and Nakamura, T., "An Evaluation of the GPS Relative Navigation System for ETS-VII and HTV," *Guidance and Control 1999*, Vol. 101, Univelt, San Diego, CA, 1999, pp. 239–257.

[10]Ebinuma, T., Bishop, R. H., and Lightsey, E. G., "Hardware-in-the-Loop GPS Test Facility for Spacecraft Autonomous Rendezvous," *ION GPS 2001* [CD-ROM], Inst. of Navigation, Fairfax, VA, 2001.

[11]Ebinuma, T., "Precision Spacecraft Rendezvous Using Global Positioning System: An Integrated Hardware Approach," Ph.D. Dissertation, Dept. of Aerospace Engineering and Engineering Mechanics, Univ. of Texas, Austin, TX, Aug. 2001.

[12]Gelb, A., *Applied Optimal Estimation*, MIT Press, Cambridge, MA, 1974, pp. 182–188.

[13]Vallado, D. A., *Fundamentals of Astodynamics and Applications*, McGraw–Hill, New York, 1997, pp. 485–497.

[14]Leick, A., *GPS Satellite Surveying*, 2nd ed., Wiley, New York, 1995, pp. 204–217.

[15]Montenbruck, O., Markgraf, M., Leung, S., and Gill, E., "A GPS Receiver for Space Application," *ION GPS 2001* [CD-ROM], Inst. of Navigation, Fairfax, VA, 2001.

[16]Leung, S., Montenbruck, O., and Bruninga, B., "Hot Start of GPS Receivers for LEO Microsatellites," *NAVITECH 2001* [CD-ROM], ESA-WPP 197, ESA Headquarters, Paris, 2001.